JCI The Journal of Clinical Investigation

Persistent *G. lamblia* impairs growth in a murine malnutrition model

Luther A. Bartelt, … , Steven Singer, Richard Guerrant

J Clin Invest. 2013;123(6):2672-2684. https://doi.org/10.1172/JCI67294.

Research Article

Giardia lamblia infections are nearly universal among children in low-income countries and are syndemic with the triumvirate of malnutrition, diarrhea, and developmental growth delays. Amidst the morass of early childhood enteropathogen exposures in these populations, *G. lamblia*–specific associations with persistent diarrhea, cognitive deficits, stunting, and nutrient deficiencies have demonstrated conflicting results, placing endemic pediatric giardiasis in a state of equipoise. Many infections in endemic settings appear to be asymptomatic/subclinical, further contributing to uncertainty regarding a causal link between *G. lamblia* infection and developmental delay. We used *G. lamblia* H3 cyst infection in a weaned mouse model of malnutrition to demonstrate that persistent giardiasis leads to epithelial cell apoptosis and crypt hyperplasia. Infection was associated with a Th2-biased inflammatory response and impaired growth. Malnutrition accentuated the severity of these growth decrements. Faltering malnourished mice exhibited impaired compensatory responses following infection and demonstrated an absence of crypt hyperplasia and subsequently blunted villus architecture. Concomitantly, severe malnutrition prevented increases in $B220^+$ cells in the lamina propria as well as mucosal *Il4* and *Il5* mRNA in response to infection. These findings add insight into the potential role of *G. lamblia* as a "stunting" pathogen and suggest that, similarly, malnourished children may be at increased risk of *G. lamblia*–potentiated growth decrements.

 Related Attending Physician, page 2346, and related Commentary, page 2352

Persistent *G. lamblia* impairs growth in a murine malnutrition model

Luther A. Bartelt,[1,2] James Roche,[1,2] Glynis Kolling,[1] David Bolick,[1] Francisco Noronha,[1] Caitlin Naylor,[1] Paul Hoffman,[1] Cirle Warren,[1] Steven Singer,[3] and Richard Guerrant[1]

[1]Division of Infectious Diseases and Center for Global Health and [2]Division of Gastroenterology, University of Virginia, Charlottesville, Virginia, USA. [3]Department of Biology, Georgetown University, Washington, DC, USA.

***Giardia lamblia* infections are nearly universal among children in low-income countries and are syndemic with the triumvirate of malnutrition, diarrhea, and developmental growth delays. Amidst the morass of early childhood enteropathogen exposures in these populations, *G. lamblia*–specific associations with persistent diarrhea, cognitive deficits, stunting, and nutrient deficiencies have demonstrated conflicting results, placing endemic pediatric giardiasis in a state of equipoise. Many infections in endemic settings appear to be asymptomatic/subclinical, further contributing to uncertainty regarding a causal link between *G. lamblia* infection and developmental delay. We used *G. lamblia* H3 cyst infection in a weaned mouse model of malnutrition to demonstrate that persistent giardiasis leads to epithelial cell apoptosis and crypt hyperplasia. Infection was associated with a Th2-biased inflammatory response and impaired growth. Malnutrition accentuated the severity of these growth decrements. Faltering malnourished mice exhibited impaired compensatory responses following infection and demonstrated an absence of crypt hyperplasia and subsequently blunted villus architecture. Concomitantly, severe malnutrition prevented increases in B220$^+$ cells in the lamina propria as well as mucosal *Il4* and *Il5* mRNA in response to infection. These findings add insight into the potential role of *G. lamblia* as a "stunting" pathogen and suggest that, similarly, malnourished children may be at increased risk of *G. lamblia*–potentiated growth decrements.**

Introduction

Giardia lamblia is an environmentally ubiquitous protozoan and one of the most common enteric parasites infecting humans worldwide (1, 2). In some low-income countries more than 90% of children have experienced at least one bout of *Giardia* infection prior to 1 year of age (3). Transmission occurs after ingestion of chlorine-resistant cysts, which undergo excystation in the duodenum and differentiation into replicating trophozoites that adhere to intestinal epithelial cells but do not invade the mucosa (4).

Malabsorptive diarrhea, nausea, abdominal cramping, flatus, and weight loss are hallmarks of symptomatic disease, though strikingly, most children in endemic settings shed cysts without overt symptoms. Despite numerous epidemiological studies, the host, pathogen, and environmental factors influencing *G. lamblia* outcomes remain incompletely defined. Investigations of equal validity have yielded conflicting results. Supporting the notion that there is an impact on developmental delay, early childhood giardiasis is associated with persistent diarrhea (5), which is a major risk factor for childhood stunting (height-for-age Z score [HAZ] of less than –2) (6). While in some studies stool carriage of *G. lamblia* is a strong predictor of either wasting or stunting (7–9), other studies of equal validity demonstrate no association between giardiasis and childhood growth (10). While Goto et. al. showed that the presence of anti–*G. lamblia* IgM (GSIgM) antibodies was associated with wasting (weight-for-age Z score [WAZ] of less than –2), but not with stunting (11), their follow-up intervention study showed no association between GSIgM antibodies and anthropometric outcomes, despite a high prevalence of recurrent infection (12). Early giardiasis has been associated with delayed psychomotor development (13) and impaired cognition (14). One or more episodes of *G. lamblia* infection in the first 2 years of life was associated with poor cognitive function at 9 years of age, independent of stunting (15). In other investigations, *G. lamblia* infection was not sufficient to explain long-term growth faltering (16). With regard to "asymptomatic" giardiasis, there are also conflicting reports of positive (17) or no correlation with longitudinal stunting (18, 19). Active *G. lamblia* infection has also been associated with vitamin A (20) and zinc deficiency (21, 22) and malnutrition in general (23). Using lactulose/mannitol ratios as a biomarker of increased intestinal permeability, Goto et. al. demonstrated a relationship between *G. lamblia* during early childhood and gut dysfunction (24), suggesting the potential for intestinal pathology concomitant with infection. Conversely, the presence of *G. lamblia* in children has been associated with an increased time to the first episode of any diarrheal event, an effect that was eliminated after multinutrient supplementation (18). A recent systematic review and meta-analysis of endemic pediatric giardiasis concluded that there is an apparently paradoxical association with protection from acute diarrhea, yet an increased risk of persistent diarrhea (25). Given the state of equipoise for this nearly universal parasite, it is important to more carefully examine *Giardia*-nutrition interactions, which are likely complex and have paramount importance in clinical outcomes.

Recent in vivo murine models of acute *G. lamblia* have demonstrated CD4$^+$-dependent parasite clearance (26, 27), CD4$^+$- and CD8$^+$-dependent brush boarder disaccharidase deficiency (27), and mast cell–induced hypermotility (28), suggesting a significant component of cellular-mediated immunopathogenesis. No studies, however, have thoroughly investigated the impact of malnutrition on outcomes following *G. lamblia* infection in weaned mice whose growth curves more closely resemble the rapid growth

Conflict of interest: The authors have declared that no conflict of interest exists.
Citation for this article: *J Clin Invest.* 2013;123(6):2672–2684. doi:10.1172/JCI67294.

in early childhood. Using *G. lamblia* cysts, Leitch et. al demonstrated that malnutrition by protein deprivation (PD) led to growth impairment in infected gerbils; however, growth curves for uninfected controls were not reported (29). More recently, Shukla et al. showed growth impairment in BALB/c mice infected with axenic trophozoites, although infection did not worsen the growth impact of PD compared with controls (30). We have previously demonstrated that malnutrition using a low-protein (LP) diet worsens growth after infection with enteroaggregative *E. coli* and *Cryptosporidium* in both neonatal and weaned murine models (31–34). We have seen from these studies that malnutrition leads to heavier infection and increased proinflammatory signaling, while infection leads to further weight faltering, thus replicating a "vicious cycle" of malnutrition and intestinal infection (31–34).

In the present study, we tested the hypothesis that persistent *G. lamblia* infection would lead to impaired growth in infected animals in a weaned murine model of infection, and that malnutrition would further exacerbate disease. We show that growth impairment and villus blunting following *G. lamblia* infection are enhanced during malnutrition, despite a similar tissue parasite burden. Using *G. lamblia* H3 cysts, we demonstrate that during persistent infection there is robust inflammatory response characterized by a predominance of mucosal eosinophils (Siglec-F$^+$) and B220$^+$ cells. Malnourished infected mice demonstrate weaker inflammatory responses to infection. Moreover, whereas malnutrition alone alters the CD4$^+$/CD8$^+$ ratio in the lamina propria compartment, *G. lamblia* infection restores this ratio in malnourished mice. We conclude that malnutrition impairs host mucosal responses that are otherwise associated with villus regeneration and relative preservation of growth after *G. lamblia* infection, and suggest that similarly, malnourished children may be at risk for *G. lamblia*–associated developmental delays.

Results

In vivo model of persistent G. lamblia demonstrates impaired growth and is associated with crypt hyperplasia and eosinophil infiltration. Whereas children in settings endemic for *Giardia* experience recurrent/persistent infections (35), previous murine models using *G. lamblia* axenic trophozoites have shown that peak parasite burden in WT mice occurs at 5 days postinfection (dpi) (27), with infection detectable only by culture of intestinal contents at 21 dpi (36). Decreased growth in infected animals, however, was not phenotypic of *G. lamblia* challenge in acute infection (S. Singer, personal communication). We hypothesized, therefore, that growth impairment more likely occurred following prolonged *G. lamblia* infection, which may be achieved using *G. lamblia* cysts, the transmissible and infective form in human disease. We challenged 5-week-old C57BL/6 males with 1×10^6 *G. lamblia* H3 cysts and monitored the animals for growth through 64 dpi. Three mice were sacrificed on 8 dpi, and excystation of *G. lamblia* was confirmed using light microscopy and visualization of motile trophozoites juxtaposed to the epithelial cell brush border in a 4-cm segment of upper small bowel (Supplemental Figure 1A; supplemental material available online with this article; doi:10.1172/JCI67294DS1). Concomitantly, *G. lamblia* cysts were seen in pooled cecal homogenates using immunofluorescence, thus confirming the presence of both stages of the parasite in their expected anatomical locations (Supplemental Figure 1B). Real-time PCR using the 18S-rRNA gene target was used for precise quantification of parasite burden in all tissue specimens with a standard curve of *G. lamblia* cysts spiked into *Giardia*-free mouse stool. For these investigations, the data are represented as "DNA copies per gram of stool (or tissue)." As defined henceforth, 1 "DNA copy" refers to the DNA content of either 1 cyst (4 nuclei per cyst) or 2 nonreplicating trophozoites (2 nuclei per trophozoite). Parasite burden in the duodenum was similar at both 8 and 64 dpi (mean ± SEM, DNA copies per gram; $1.225 \times 10^7 \pm 4.560 \times 10^6$ vs. $1.353 \times 10^7 \pm 7.868$, respectively; $P = 0.7079$). Parasites were more numerous in the duodenum than in the ileum at both time points ($P = 0.0314$ at 8 dpi and $P = 0.0006$ at 64 dpi) (Figure 1A). Decreased growth in infected mice compared with controls began at 35 dpi, reached a maximum difference at 42 dpi (average Δ weight grams, 4.7325 vs. 5.422; $P < 0.05$), and showed partial recovery by 64 dpi (Figure 1B). Histological morphometry confirmed crypt hyperplasia in infected mice (mean depth ± SEM mm, 122.5 ± 5.784 vs. 101.4 ± 4.940, respectively; $P = 0.0266$) with preserved villus length (mean depth ± SEM mm 663.7 ± 19.08 vs. 674.7 ± 11.84, respectively; $P = 0.6234$), and decreased villus height/crypt depth ratio (mean depth ± SEM 5.345 ± 0.5305 vs. 6.799 ± 0.2242, respectively $P = 0.0290$) (Figure 1, C–K). The lamina propria appeared expanded, and intraepithelial eosinophils were greater in both the villus (mean eosinophils ± SEM, 8.450 ± 1.052 vs. 2.900 ± 1.052; $P = 0.0008$) and crypt epithelium (mean eosinophils ± SEM, 7.075 ± 1.264 vs. 2.800 ± 0.5925; $P = 0.0132$) of infected mice compared with controls (Figure 1L).

G. lamblia H3 cyst infection is associated with further decreased growth and persistent parasite shedding in malnourished mice. Unlike WT C57BL/6 mice, IL-6 and CD4$^+$ T cell–deficient mice have impaired clearance of *G. lamblia* trophozoites (26, 37). We hypothesized that malnourished, weaned C57BL/6 mice would also have impaired clearance due to malnutrition-related immunosuppression. To test this hypothesis, we malnourished mice using an LP deprivation diet (2% protein), similar to our previously published protocols for *Cryptosporidium* infections (33, 34). We infected 3-week-old mice after 8 days of LP preconditioning with 1×10^7 WB axenic trophozoites (assemblage A by *Tpi* sequencing, data not shown), 1×10^6 *G. lamblia* H3 cysts (assemblage B by *Tpi* sequencing, data not shown), or PBS challenge as a control. Serial stool samples revealed that infection with WB trophozoites was readily cleared, whereas shedding increased in the second week following challenge with H3 cysts ($P < 0.001$, 11–15 dpi) (Figure 2A). We observed a heavy burden of parasites in the small bowel tissue at 15 dpi in only the H3 cyst–infected mice, which was greater in the duodenum (mean ± SEM DNA copies per gram, $1.995 \times 10^7 \pm 1.026 \times 10^7$) and decreased distally throughout the small intestine (mean ± SEM parasites per gram, $1.218 \times 10^6 \pm 9.176 \times 10^5$, jejunum, $P = 0.0398$; $4.228 \times 10^4 \pm 1.621 \times 10^4$, ileum, $P < 0.0001$; $2.149 \times 10^6 \pm 9.359 \times 10^5$, cecum, $P = 0.0681$) (Figure 2B). Furthermore, growth impairment compared with controls was seen only in the *G. lamblia* H3 cyst–challenged mice ($P < 0.05$, 12 dpi versus trophozoites; $P < 0.01$, 15 dpi versus trophozoites) (Figure 2C), and compared with our earlier observation in infected nourished mice, growth impairment occurred 3 weeks sooner in the malnourished mice. Thus, whereas the malnourished (LP-fed) mice were capable of clearing axenic WB trophozoites in an expected time course, there was accentuated growth impairment concomitant with persistent detectable parasite burden in the *G. lamblia* H3 cyst infection model.

Prolonged malnutrition alters mucosal architecture following G. lamblia infection. To investigate whether the duration of malnutrition further influenced growth during infection, 3-week-old mice were either infected or PBS challenged after 8 days of

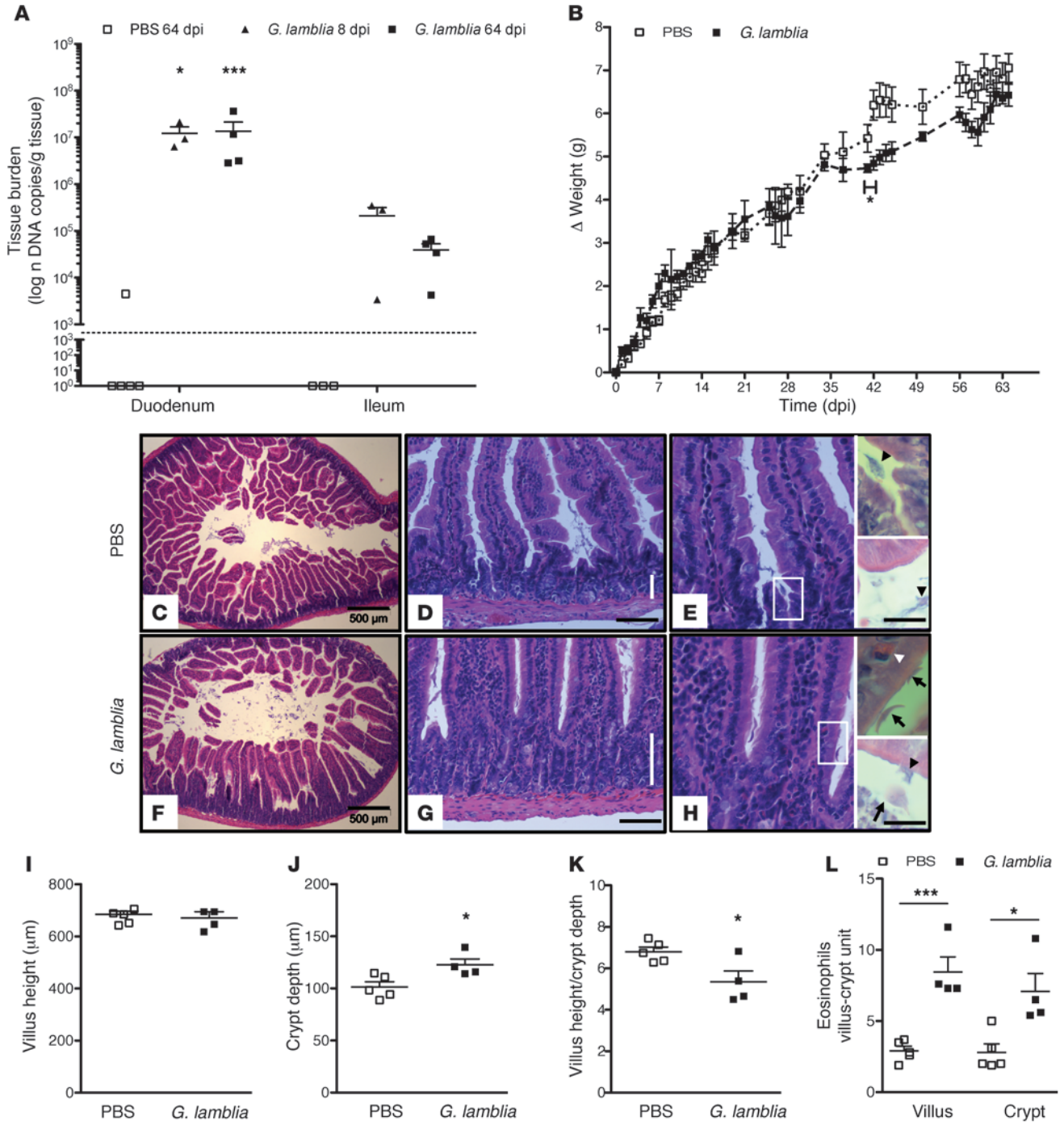

Figure 1

Persistent *G. lamblia* infection in nourished mice is associated with impaired growth, eosinophil infiltration, and crypt hyperplasia. (**A**) *G. lamblia* tissue burden determined by qPCR in duodenum compared with ileum at 8 and 64 dpi (n = 3–5 per group). The dashed line represents the PCR limit of detection. *P = 0.029; ***P = 0.001. (**B**) Growth curves measuring the change in weight after challenge with PBS (n = 5) or 10^6 *G. lamblia* (n = 4) as indicated (*P < 0.05, day 42). (**C**–**E**) Representative H&E-stained duodenum sections of a single PBS-challenged mouse at 64 days after challenge. Vertical bar represents crypt depth (**D**). Black arrowhead represents mucus. Scale bars: 500 (**C**), 100 (**D**), and 50 microns (**E**) (inset, 20 microns). (**F**–**H**) Representative H&E-stained duodenum sections of a single *G. lamblia*–infected mouse at 64 dpi. Vertical bar represents crypt depth (**G**). Scale bars: 500 (**C**), 100 (**D**), and 50 microns (**E**). (**H**) Representative H&E-stained duodenum section at 64 days after challenge with *G. lamblia* showing hypercellularity in the crypts and villus base. Arrows indicate *G. lamblia* in ventral (lower right) and transverse (upper right) orientations, white arrowhead represents an intraepithelial eosinophil, and black arrowhead represents mucus. Scale bar: 50 microns (inset, 20 microns). (**I**–**K**) Mucosal morphometric changes at 64 dpi measured on H&E-stained duodenum sections. Original magnification, ×10. (**J**) *P = 0.027; (**K**) *P = 0.029. (**L**) Enumeration of eosinophils on ×20 H&E-stained duodenum sections in PBS-challenged and *G. lamblia*–challenged mice at 64 dpi. *P = 0.013; ***P < 0.001.

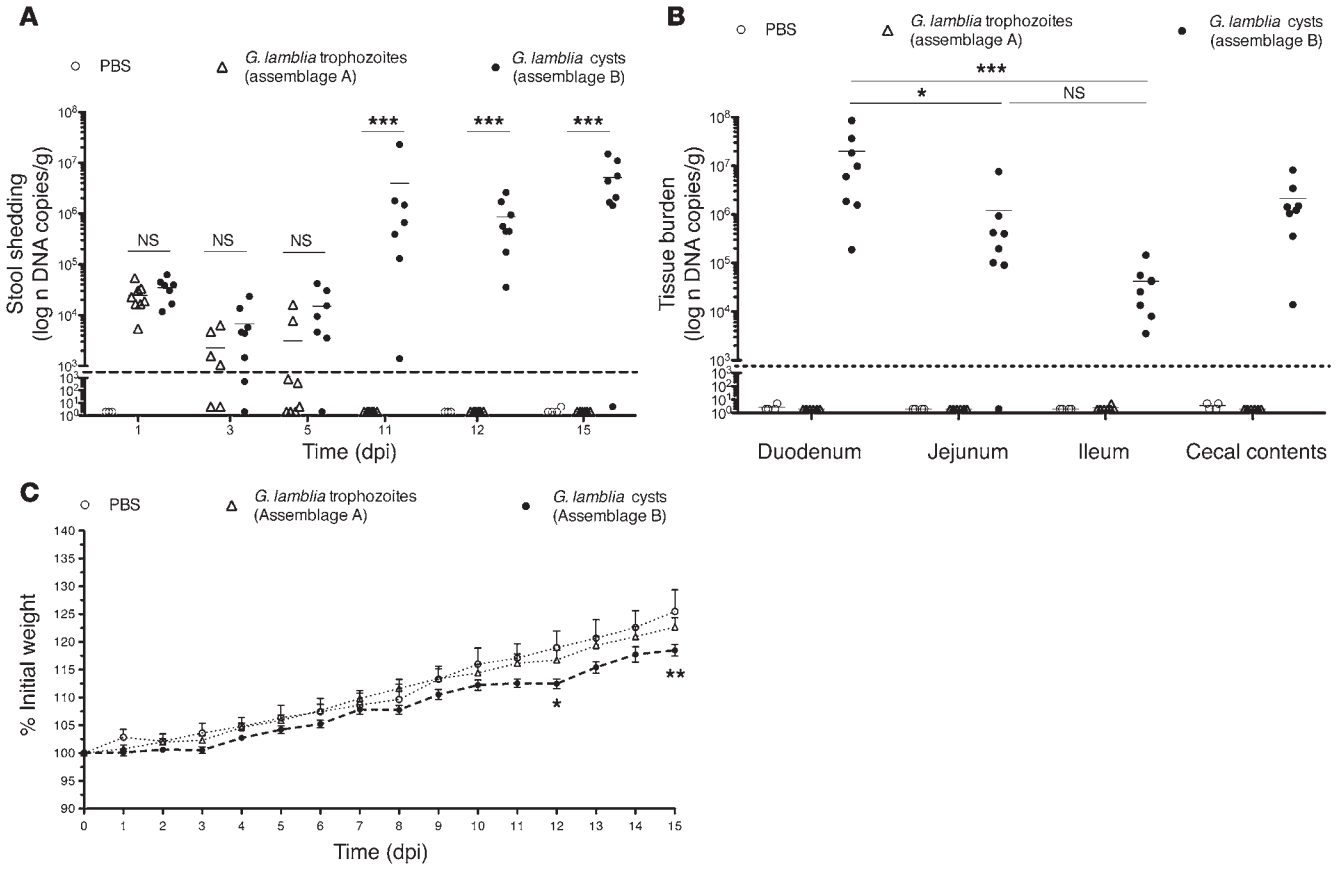

Figure 2

Challenge with *G. lamblia* H3 cysts in malnourished mice is persistent and is associated with early growth faltering. (**A**) *G. lamblia* serial stool shedding determined by qPCR on indicated dpi (***$P < 0.001$) and (**B**) in small bowel intestinal tissues at 15 dpi (*$P < 0.04$ and ***$P < 0.001$ vs. duodenum). Dashed line represents the limit of detection on both graphs. (**C**) Growth curves measuring the percentage of change in weight beginning on the day of infection with *G. lamblia* H3 cysts ($n = 8$), *G. lamblia* WB trophozoites ($n = 8$), or PBS control ($n = 3$; original PBS control was $n = 4$, but 1 mouse was excluded secondary to significant gavage trauma and >20% weight loss by day 4). *$P = 0.05$, 12 dpi; **$P < 0.01$, 15 dpi; H3 cysts versus PBS.

LP preconditioning (experimental day 0 [D0]) or infected after 15 days of LP preconditioning (experimental day 7 [D7]). All were continued on their respective diets through 7 weeks of life (experimental day 22 [D22]), and compared with age-matched PBS-challenged or infected nourished (RP-fed) mice. Whereas infected mice on the RP diet showed uniform growth through 22 dpi, infected mice on the LP diet showed greater growth decrements compared with the uninfected LP-fed controls (Figure 3A). Mice that underwent a longer duration of malnutrition prior to infection (LP-fed, challenged on D7), however, demonstrated earlier and more significant growth impairment compared with the LP-fed uninfected controls ($P < 0.0001$) (Figure 3B). The intensity of parasite burden in the stool was similar irrespective of diet (Figure 3C). Thus, the RP-fed mice had no better clearance of infection, yet the LP-fed mice were more susceptible to growth faltering at a similar parasite burden. Intestinal tissue burden showed a predominance of *G. lamblia* in the duodenum and the cecum (Figure 3D) for all infected groups. At 22 dpi, duodenal and jejunal tissue burden was similar regardless of diet (mean ± SEM DNA copies per gram; $9.059 \times 10^7 \pm 5.164 \times 10^7$ RP-fed vs. $1.945 \times 10^8 \pm 1.252 \times 10^7$ LP-fed; $P = 0.4791$), and cecal tissue burden was greater in RP-fed mice compared with LP-fed mice (mean ± SEM DNA copies per gram; $2.422 \times 10^6 \pm 1.519 \times 10^6$ vs. $2.297 \times 10^5 \pm 1.214 \times 10^5$, respectively; $P < 0.0037$) (Figure 3D).

To further investigate the mucosal responses to infection and malnutrition, we examined duodenal tissues from the same RP- and LP-preconditioned mice (LP: *G. lamblia* D0, 22 dpi) at 22 dpi and prolonged LP-preconditioned mice (LP: *G. lamblia* D7, 15 dpi) at 15 dpi. Consistent with the changes seen at 64 dpi (see Figure 1), *G. lamblia* infection in RP-fed mice was associated with altered villus height/crypt depth ratios (mean ± SEM μm; 8.683 ± 0.3740, controls vs. 6.198 ± 0.3715, *G. lamblia*; $P = 0.001$) and crypt hyperplasia compared with RP-fed controls (mean ± SEM μm 97.58 ± 3.672, *G. lamblia* vs. 66.22 ± 2.936, controls; $P < 0.001$) (Figure 4, A–E). LP-fed control mice compared with RP-fed control mice demonstrated decreased villus height/crypt depth ratios (mean ± SEM μm; 7.134 ± 0.5578 vs. 8.683 ± 0.3740, respectively; $P = 0.05$), with blunted villi (mean ± SEM μm; 437.5 ± 16.62 LP-fed vs. 564.2 ± 34.47 RP-fed; $P = 0.0078$), but similar crypt depths (Figure 4, A–D, and F). Prolonged LP-preconditioned (LP: *G. lamblia* D7, 15 dpi) mice had significant villus blunting after infection compared with LP-fed controls (mean ± SEM μm; 368.2 ± 22.98 vs. 437.5 ± 16.62, respectively; $P = 0.0365$) and a greater reduction in villus height/crypt

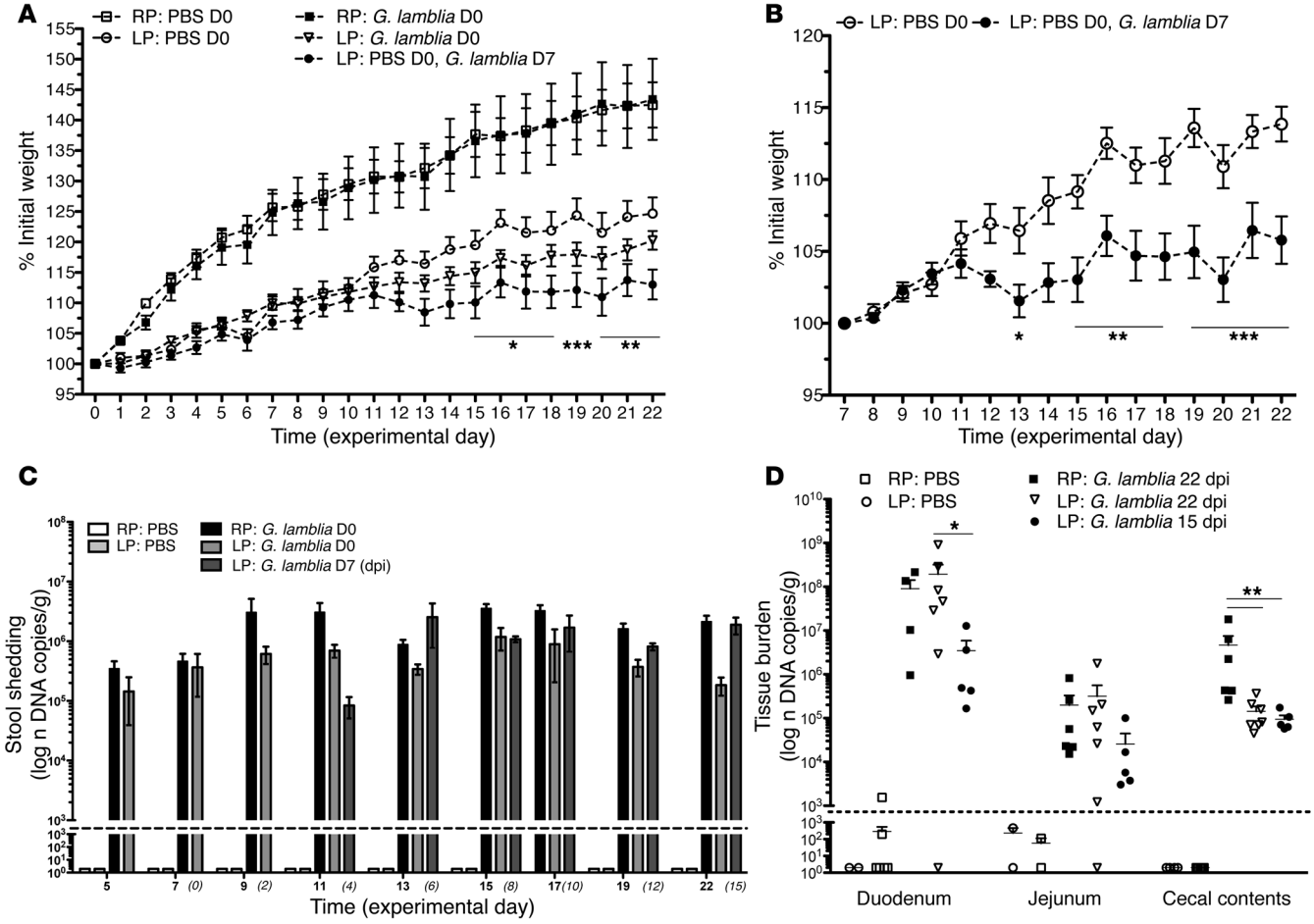

Figure 3

G. lamblia–associated growth faltering is accentuated with more prolonged malnutrition. (**A**) Growth curves measuring the percentage of initial weight following a 20% protein diet (RP) or a 2% protein diet (LP). Day 0 is the day of infection with *G. lamblia* H3 cysts or PBS challenge. One group of mice challenged with PBS on day 0 (D0) was challenged with *G. lamblia* H3 cysts on day 7 (D 7) (n = 5–7). $P < 0.05$, RP: PBS vs. LP: PBS; *$P < 0.05$, **$P < 0.01$, ***$P < 0.001$, LP: PBS vs. LP: *G. lamblia* D7. (**B**) Growth curves showing percentage of initial weight change beginning 15 days after initiation of an LP diet. Day 7 is the day of infection. *$P < 0.05$; **$P < 0.01$; ***$P < 0.001$. (**C**) Parasite burden determined by qPCR in serial stool collections on indicated dpi and (**D**) in representative intestinal tissues 15 dpi (infected on day 7) and 22 dpi (infected on day 0). *$P = 0.006$; **$P < 0.001$. Dashed line represents the limit of detection on both graphs.

depth ratios (mean ± SEM μm; 5.386 ± 0.3282 vs. 7.134 ± 0.5578, respectively; $P = 0.0467$). Mice infected after 8 days on an LP diet (LP: *G. lamblia* D0, 22 dpi) demonstrated mucosal architecture that was intermediate compared with the LP PBS–treated and prolonged LP-preconditioned mice (LP: *G. lamblia* D7, 15 dpi) (Figure 4, A–C, and F–H).

G. lamblia NF and S2 axenic trophozoites have been shown to induce apoptosis through the caspase-3 pathway in vitro (38), and similarly, increased apoptotic epithelial cells were seen in jejunal biopsies of patients with chronic giardiasis (39). We confirmed that *G. lamblia* H3 cysts in RP-fed mice were associated with increased cleaved caspase-3 antibody staining in both the villi and crypts compared with the distribution seen primarily at the terminal villus epithelial cells in the controls (mean ± SEM cells per villus-crypt unit 2.718 ± 0.5453 vs. 1.024 ± 0.1899, respectively; $P = 0.0150$) (Figure 4, I–K). LP-fed mice did not, however, demonstrate an increased frequency of cleaved caspase-3 staining, irrespective of infection (Figure 4K).

Malnutrition blunts eosinophil infiltration and IL4 and IL5 expression following G. lamblia infection. Humans demonstrate variable immune responses to *G. lamblia* infections, including approximately 30% of jejunal biopsies from infected children that show increased eosinophils (40). Histopathological staining of duodenal tissues at 22 dpi in both RP-fed and LP-fed infected mice and 15 dpi in the LP-fed mice demonstrated increased intraepithelial eosinophils in crypts (mean ± SEM cells per villus-crypt unit; 7.717 ± 1.082, RP-fed *G. lamblia* vs. 1.550 ± 0.1384 RP-fed control mice, $P < 0.001$; 5.033 ± 0.6259 LP-fed *G. lamblia* mice 22 dpi vs. 1.500 ± 0.1571 LP-fed control mice, $P < 0.001$; 5.220 ± 0.7703 LP-fed *G. lamblia* mice 15 dpi vs. 1.500 ±.1571 LP-fed control mice, $P < 0.001$), and in villi (mean ± SEM cells per villus-crypt unit; 7.950 ± 1.636 RP-fed *G. lamblia* mice vs. 2.083 ± 0.2915 RP-fed control mice, $P = 0.0054$; 4.967 ± 0.8065 LP-fed *G. lamblia* mice 22 dpi vs. 2.600 ± 0.4450 LP-fed control mice, $P = 0.0279$; 4.160 ± 0.5776 LP-fed *G. lamblia* mice 15 dpi vs. 2.600 ± 0.4450 LP-fed control mice, $P = 0.0575$) compared with controls (Figure 4,

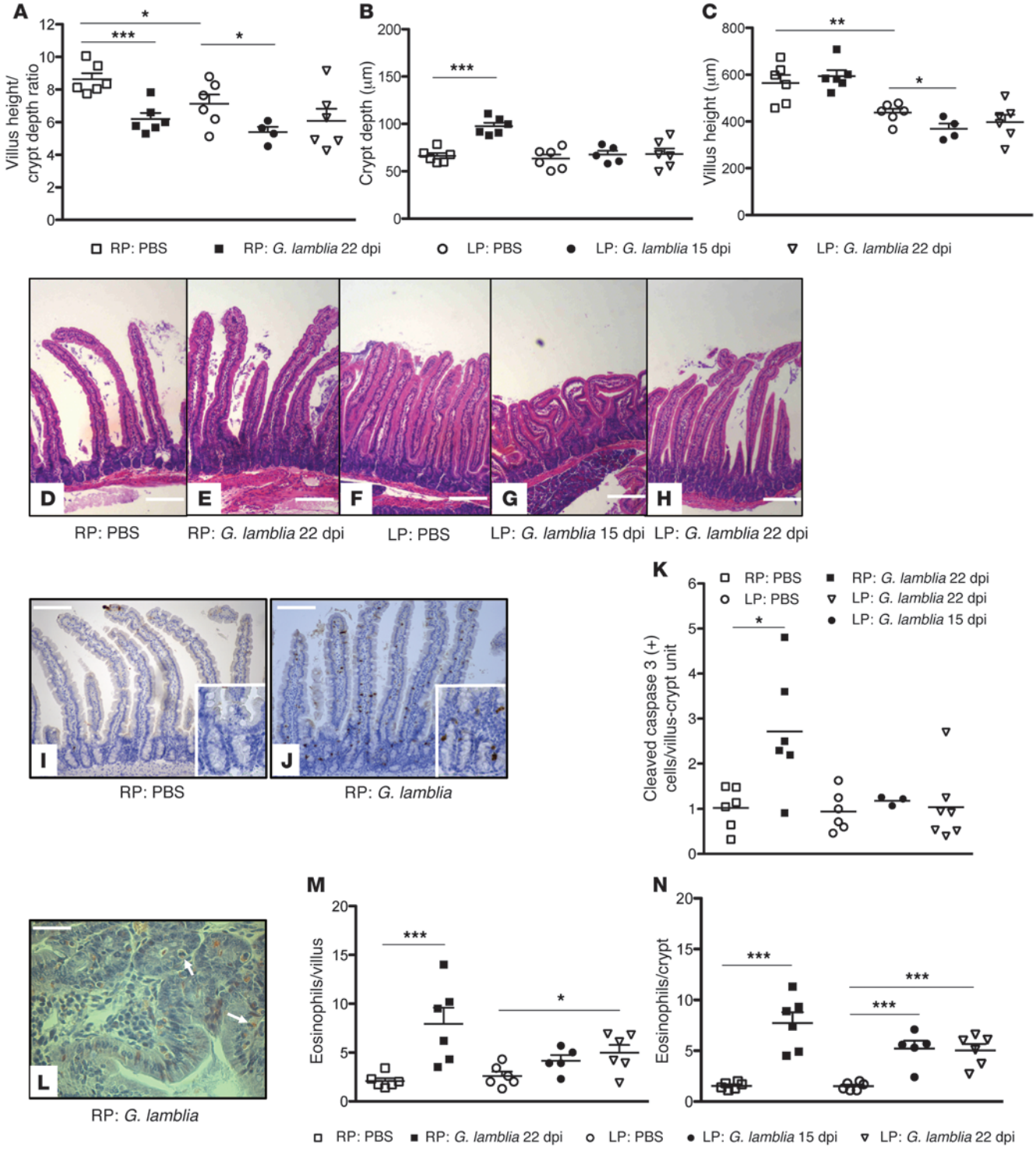

Figure 4

Malnutrition diminishes apoptosis, crypt hyperplasia, and eosinophil responses to *G. lamblia* infection. (**A**–**C**) Villus and crypt architectural changes following *G. lamblia* infection in RP- and LP-fed mice at indicated time points after infection (n = 4–7 mice per group). Bar caps designate comparisons. *P < 0.05; **P < 0.01; ***P < 0.001 for all graphs. (**D**–**H**) Representative H&E-stained sections of a single mouse from each group as indicated. Images were selected to best represent the average morphometry in each group. Scale bars: 500 microns. (**I** and **J**) Cleaved caspase-3 immunohistochemistry staining as indicated. Scale bars: 200 microns (inset, 100 microns) (**K**) Number of cells positive for cleaved caspase-3 staining per villus-crypt unit. Original magnification, ×20. *P = 0.015. Representative cleaved caspase-3 immunohistochemically stained intestinal sections as indicated. (**L**) Congo red stain demonstrating eosinophils within the epithelium of *G. lamblia*–infected RP-fed mouse. (**M** and **N**) Enumeration of eosinophils on H&E staining at ×20 and ×40 magnification per villus or crypt as indicated. Bar caps designate comparisons. *P = 0.026; **P < 0.01; ***P < 0.001.

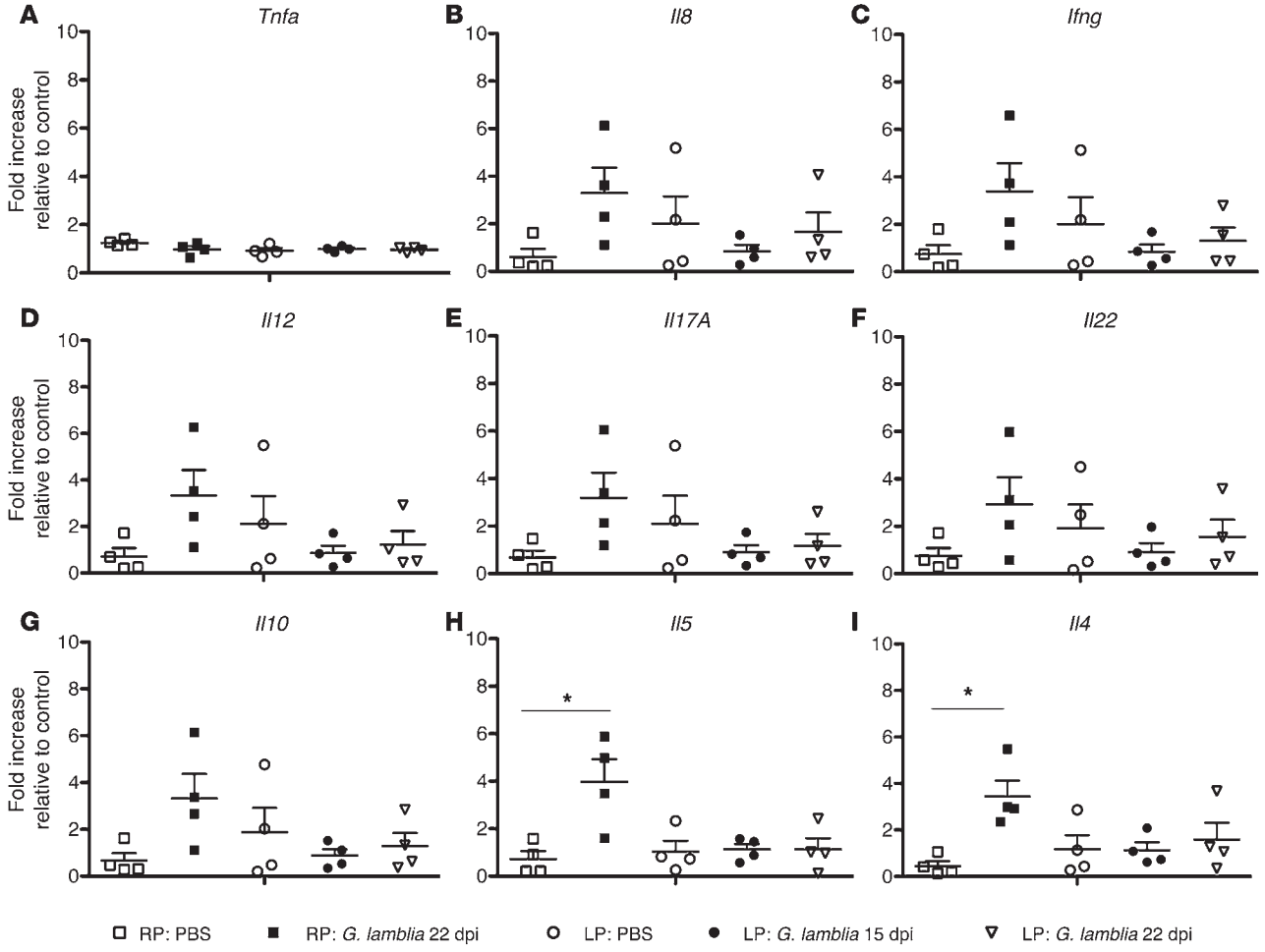

Figure 5

G. lamblia is associated with significantly elevated tissue expression of *Il4* and *Il5* mRNA at 22 dpi, and malnutrition blunts this response. Fold change increase in duodenal cytokine mRNA expression normalized to the geometric mean of beta-actin and HPRT relative to controls (RP: PBS) for (**A**) *Tnfa*, (**B**) *Il8* (CXCR1/KC), (**C**) *Ifng*, (**D**) *Il12*, (**E**) *Il17a*, (**F**) *Il22*, (**G**) *Il10*, (**H**) *Il5*, and (**I**) *Il4*. **P* < 0.05.

L–N). Although not statistically significant, the magnitude of eosinophil infiltration in the RP-fed infected mice was greater than that in the LP-fed infected mice.

In longitudinal studies of children in Mexico, stool cytokine analysis showed that children who failed to clear *Giaridia* had increased IL-4, IL-5, MCP1, and IFN-γ, and decreased IL-8 (41). Observing that eosinophils were increased, we proceeded to investigate mRNA cytokine profiles in matched mouse duodenal tissues (Figure 5, A–I). The quantity of each cytokine was normalized for each individual sample relative to the geomean of the housekeeping genes (beta-actin and *HPRT*), and is expressed as the fold change increase relative to RP PBS controls. *G. lamblia* infection in RP-fed mice is associated with significantly elevated mRNA expression of *Il5* (mean ± SEM fold increase; 3.983 ± 0.9356 vs. 0.7225 ± 0.3312, respectively; $P < 0.05$) and *Il4* (mean ± SEM fold increase; 3.438 ± 0.6953 vs. 0.4550 ± 0.2105, respectively; $P < 0.05$) relative to controls (RP: PBS), whereas infection in LP-fed mice is not (Figure 5, H and I).

Malnutrition alters lamina propria T cell CD4⁺/CD8⁺ ratio and impairs B cell responses to G. lamblia. Impairments in both cellular and humoral immunity have been documented in malnourished children (42), and 2 weeks of malnutrition was adequate to impair antibody responses to cholera toxin in protein-deprived rats (43). To further explore the alterations in immune responses subsequent to malnutrition and *G. lamblia* H3 infection, we performed flow cytometry on upper small bowel at 21 dpi (8 weeks of age) in both nourished (RP-fed) and malnourished (LP-fed, 15 days of LP preconditioning prior to challenge) mice (Figure 5, H and I). A single-stain analysis of epithelial and lamina propria fractions was performed using an initial side scatter and forward scatter gating strategy to isolate leukocytes (Supplemental Figure 2). We observed marked differences in the immune responses to infection between the nourished and malnourished mice. Within the epithelial fraction, *G. lamblia* infection in RP-fed mice was associated with an increased frequency of eosinophils (Siglec-F⁺) (mean ± SEM; 10.64 ± 1.644 vs. 3.190 ± 0.4067, respectively; $P = 0.01$) and B cells (B220⁺) (mean ± SEM; 13.90 ± 1.872 vs. 6.410 ± 1.072, respectively; $P = 0.0255$) (Figure 6A). Eosinophils were also increased in the malnourished (LP-fed) infected mice (mean ± SEM; 7.107 ± 1.423 vs. 2.673 ± 0.05239; $P = 0.0357$), though to a lesser degree than in the nourished infected mice (Figure 6A). Whereas malnutrition (LP-fed) without infection was associated with increased B220⁺

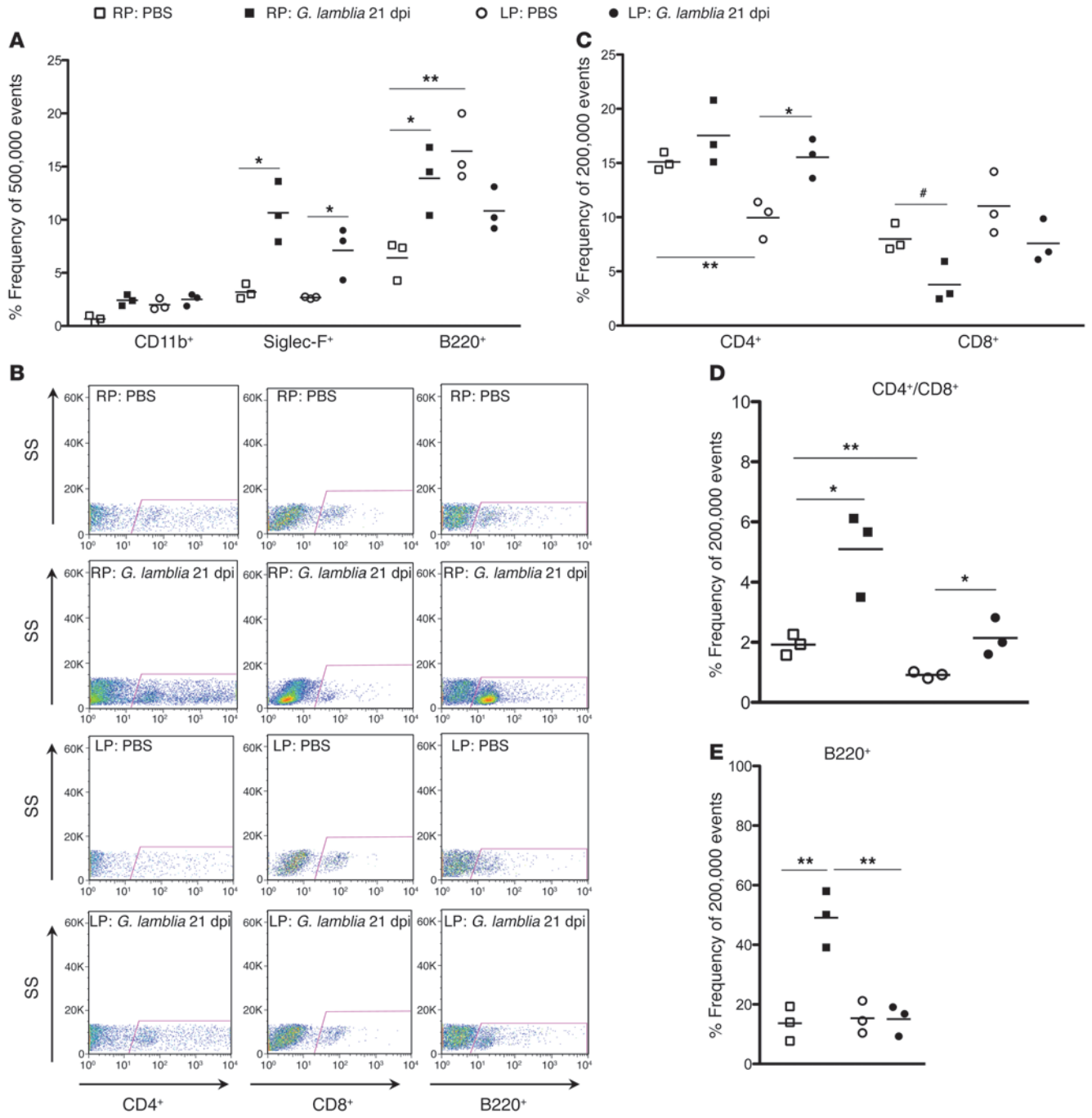

Figure 6

Both *G. lamblia* and malnutrition alter the relative frequencies among lymphocyte populations in the lamina propria, and *G. lamblia* increases eosinophils and B cells in the epithelium. Flow cytometry of epithelium and lamina propria fractions taken 22 dpi with 10^6 *G. lamblia* H3 cysts. (**A**) Epithelial fraction, $^*P < 0.05$, $^{**}P = 0.009$. (**B**) Representative flow cytometry of lamina propria lymphocytes (LPLs) as side scatter (SS) versus CD4+, CD8+, or B220+ as designated. (**C**) LPL T cell population frequencies as designated. $^*P = 0.019$; $^{**}P < 0.011$; $^{\#}P < 0.033$. (**D**) LPL CD4+/CD8+ ratios. $^*P < 0.05$; $^{**}P = 0.008$. (**E**) LPL B cell (B220+) frequencies. $^{**}P = 0.005$.

cells in the epithelial compartment compared with the nourished (RP-fed) controls (mean ± SEM; 16.43 ± 1.811 vs. 6.410 ± 1.072, respectively; $P = 0.0089$), *G. lamblia* infection in malnourished (LP-fed) mice was associated with a decrease in the number of B220+ cells compared with the LP-fed controls (mean ± SEM; 10.83 ± 1.174 vs. 16.43 ± 1.811, respectively; $P = 0.0602$).

Flow cytometry within the lamina propria (Figure 6B) demonstrated that, compared with nourished (RP-fed) control mice, malnourished (LP-fed) controls had a decreased frequency of CD4+ cells per 200,000 leukocyte events (mean ± SEM; 9.953 ± 1.030 vs. 15.10 ± 0.4726, respectively; $P = 0.01015$), with preserved CD8+ cells (mean ± SEM; 11.03 ± 1.660 vs. 7.993 ± 0.7407, respectively;

$P = 0.1701$ (Figure 6C) and a resultant decrease in the normal $CD4^+/CD8^+$ ratio (mean ± SEM, 0.9163 ± 0.06258 vs. 1.923 ± 0.1978, respectively; $P = 0.0083$) (Figure 6D). Malnutrition alone did not result in differences in the number of lamina propria $B220^+$ cells (Figure 6E). *G. lamblia* challenge at 21 dpi, however, showed the RP-fed mice to have a 3.6-fold increase in $B220^+$ cells compared with the RP-fed controls (mean ± SEM; 49.07 ± 0.5.480 vs. 13.66 ± 3.356, respectively; $P = 0.0053$), no significant change in $CD4^+$ cells (mean ± SEM; 17.53 ± 1.697 vs. 15.10 ± 0.4726, respectively; $P = 0.2394$), and a relative decrease in $CD8^+$ cells (mean ± SEM; 3.787 ± 0.1.086 vs. 7.993 ± 0.7407, respectively; $P = 0.0329$), resulting in a 2.6-fold increase in the $CD4^+/D8^+$ ratio (mean ± SEM; 5.092 ± 0.8056 vs. 1.923 ± 0.1978, respectively; $P = 0.0188$) (Figure 6, C and D). In contrast, *G. lamblia* challenge at 21 dpi in malnourished (LP-fed) mice resulted in increased $CD4^+$ cells (mean ± SEM; 15.53 ± 1.048 versus 9.953 ± 1.030, respectively; $P = 0.0191$), no significant change in $CD8^+$ cell numbers (mean ± SEM; 7.587 ± 1.154 vs. 11.03 ± 1.660, respectively; $P = 0.1638$), and a restoration of the $CD4^+/CD8^+$ ratio (mean ± SEM, 2.141 ± 0.3586 vs. 0.9163 ± 0.06258, respectively; $P = 0.0282$) (Figure 6, C and D). Furthermore, the malnourished (LP-fed) mice had no increase in lamina propria $B220^+$ cells (Figure 6E).

Discussion

We developed a murine model of persistent giardiasis using *G. lamblia* H3 (assemblage B) cysts that causes growth faltering, chronic inflammation, and alterations in mucosal morphometry overlapping with those seen in some human studies (39). The malnutrition-enhanced growth decrements observed in this model compared with similarly infected nourished mice revealed diminished mucosal type 2 cytokine responses and decreased enrichment of $B220^+$ cells in the lamina propria concomitant with villus blunting. Thus, this approach can serve as a model for studying host responses to persistent giardiasis and the impact of malnutrition on mucosal restitution as it relates to the immune responses following infection.

Results from our murine model demonstrate a compounded effect of persistent *G. lamblia* on growth outcomes in the setting of host malnutrition, an area of equipoise in epidemiological studies of early childhood infections. Although growth failure was present in nourished mice, the effect was modest and delayed relative to the more profound decrement seen in the setting of malnutrition. Counter to other enteric infections in malnutrition (32–34), this compounded effect cannot be explained by a higher burden of infection in the malnourished mice. Intriguingly, another investigation also demonstrated a relatively decreased burden of *G. lamblia* trophozoites in the small bowel following severe PD in mice (44). Rather than an increased burden of parasites, malnourished mice in our model lacked crypt hyperplasia following *G. lamblia* infection and had resultant villus blunting. We therefore focused our investigations on the compensatory host responses that, when diminished in the setting of malnutrition, could provide a mechanistic explanation accounting for the more severe disease in this group.

Like some cases of chronic human giardiasis (39), histopathology following persistent *G. lamblia* H3 infection in mice demonstrates increased markers of apoptosis in the epithelium (at 22 dpi) as well as reduced villus height/crypt depth ratio, crypt hyperplasia, and hypercellularity in the lamina propria (at 22 and 63 dpi). The immune response at these time points is characterized by a predominance of $B220^+$ cells in the lamina propria, elevated *Il4* and *Il5* mRNA, and intraepithelial eosinophils, consistent with a Th2-biased response. Similarly, markers of Th2 responses have been documented in human infections, including eosinophilic infiltrates in approximately one-third of jejunal biopsies from children (40), elevated IL-4 and IL-5 in stools of children who fail to clear *Giardia* (41), and elevated serum IL-13 following acute infection in adults (45). The mechanisms driving this response are poorly understood, and the clinical studies did not exclude the presence of coinfecting helminths, which is associated with both mucosal eosinophils and susceptibility to *G. lamblia* (46). Acute *Giardia* infection with axenic trophozoites in mice does not demonstrate a robust inflammatory response (46), consistent with in vitro findings of suppressed DC cytokine production following exposure to *Giardia* or *Giardia* products in vitro (47). *G. lamblia* contains a biologically unique β-1,3 GalNAc homopolymer in its cyst wall (48), which in our cyst challenge model could partially explain why a different immune response was seen. Interestingly, Jimenez et al. demonstrated that BALB/c mice exposed to axenic *G. lamblia* P1 trophozoite excretory-secretory (E-S) products elicited tissue eosinophilia and elevated serum IgE (49). Although further investigation is needed to conclude whether the Th-2 biased response is parasite strain– or stage-initiated, our observations raise new implications regarding host factors, such as malnutrition, that lead to worse disease outcomes when this response is blunted. Whether a subset of early childhood giardiasis that correlates with persistent diarrhea and/or growth failure demonstrates particular markers of this immune response has not been thoroughly examined, but could be considered for future investigations.

G. lamblia and host responses may have opposing effects on epithelial cells. Consistent with our finding in nourished, infected mice, in vitro studies of *G. lamblia* have demonstrated the induction of apoptosis through the caspase-3 pathway (50), and more recently, cell-cycle arrest at the G1/S phase through the deprivation of arginine from the host epithelial cell (51). Conversely, in our in vivo model, crypt hyperplasia is seen following infection in nourished mice. The latter is consistent with findings that *G. lamblia* in immunocompetent hosts is associated with $BrdU^+$ uptake in villus epithelial cells, resulting in a relative increase in immature enterocytes at the villus base, which accounted for microvillus cytoskeletal abnormalities and disaccharidase deficiency (52). The cellular and molecular signals promoting epithelial cell proliferation in giardiasis are not well defined. Our model demonstrates that increased IL-4 and IL-5, cytokines that are not elevated in malnourished, infected mice that do demonstrate villus blunting, are potentially important in compensatory host responses to *G. lamblia*.

Future investigations into the role of cytokine responses in this model can advance our understanding of the role of mucosal immune responses in villus repair following enteric infections. Th2 responses have been shown to increase epithelial cell proliferation following helminthic infections in mice (53). Diminished markers of this response in our model include a less robust increase in intraepithelial eosinophils ($Siglec\text{-}F^+$), a strikingly absent increase in $B220^+$ cells in the lamina propria, and no significant upregulation of *Il4* or *Il5* mRNA in malnourished compared with nourished mice following *G. lamblia* infection. Delineating how the host mucosal immune response affects epithelial cell proliferation will thus be critical for understanding disease pathogenesis subsequent to *Giardia*, mechanisms which may account for the variability seen in the subset of children who have associated growth failure subsequent to infection.

While our model supports a strong influence of malnutrition on disease outcomes, other factors may also account for variability in endemic giardiasis outcomes, including host genetic determinants, strain pathogenicity, and microflora, each of which represents an important future direction of investigation. Delineating how these factors influence growth outcomes in a model such as the one we have developed will be important, given the clinical challenges in investigating endemic pediatric giardiasis, where excretion of parasites without overt symptoms is common.

Host susceptibility likely contributes to disease variation in giardiasis. Known risk factors for chronic giardiasis in humans include immunoglobulin disorders (i.e., selective IgA deficiency, X-linked agammaglobulinemia [XLA], or common variable immunodeficiency [CVID]); however, few studies have thoroughly investigated the chronicity of disease in children living in endemic settings (54) where confounding environmental and pathogen-specific factors are influential. While stool IgA was not measured in this investigation, even the nourished, infected animals with large numbers of $B220^+$ cells in the lamina propria had persistent infection, suggesting that the pathogenicity of the infecting strain at least partially accounts for the persistence in this model.

To our knowledge, this is the first murine giardiasis model to use purified *G. lamblia* H3 cysts, which are otherwise primarily used for diagnostic purposes (55, 56). The cysts were acquired from Waterborne, Inc. and originated from an initial human isolate (H. Stibbs, Waterborne, Inc., personal communication). The resulting persistent infection is in stark contrast to other murine *G. lamblia* models wherein parasites progressively migrate distally in the gut (57) and are detectable only by culturing the intestinal contents within a couple of weeks (36, 58). That challenge with 10^6 H3 cysts persisted much longer than 10^7 WB (assemblage A) trophozoites is consistent with other studies demonstrating strain variability between assemblages both in vivo and in vitro (27, 50). Furthermore, human volunteer studies demonstrated variable pathogenicity within the B assemblage (59). The most widely used *G. lamblia* assemblage B strain (GS-M83-H7) has not been shown to persist in significant numbers beyond 2 weeks in WT mice in the United States (S. Singer, personal communication). Thus, additional direct comparisons between assemblage A and various assemblage B isolates in this model and in field studies will be necessary to determine the influence of strain variability on *G. lamblia* outcomes, particularly in the subset of children with growth faltering.

The use of the cyst stage of the parasite may have also influenced infectivity in our model. Due to technical challenges in encysting viable axenic trophozoites and poor in vitro growth after recultivating H3 trophozoites (data not shown), we were unable to perform a direct comparison between the H3 stages. We acknowledge that even trace amounts of contaminants in these purified H3 cysts could account for the differences seen compared with trophozoite infection models. Indeed, the influence of the microbiota on giardiasis outcomes requires future investigation, as has been proposed in probiotic intervention studies using *Lactobacillus spp.* in other murine *Giardia* models (30).

In conclusion, diarrhea concomitant with growth faltering is an ongoing affliction of malnourished children worldwide. Among the potential causative agents, *G. lamblia* is nearly universal (3), but its relative contribution to disease in endemic settings is controversial. Further confounding our understanding of the mechanisms of *G. lamblia* pathogenesis is an apparent spectrum of manifestations from asymptomatic presentation in the majority of humans, to profound wasting and developmental delay (1, 13, 14), to even potential antidiarrheal effects (18). In what we believe to be a novel murine model of persistent infection that utilizes the previously untested *G. lamblia* H3 (assemblage B) isolate, we replicated many aspects of chronic human giardiasis that herein are associated with growth failure — an outcome that is profoundly influenced by host nutritional status. We propose an early mechanistic hypothesis, whereby a lack of villus regeneration coincident with malnutrition-induced immunosuppression accounts for accentuated growth impairments in malnourished mice. While the weight of mice in this investigation is not a direct surrogate for stunting (i.e., HAZ) in children, our findings underline the importance of considering host mucosal responses as correlates of clinical outcomes in endemic pediatric giardiasis, and suggest that malnourished children may be similarly vulnerable to *Giardia*-related developmental growth sequelae.

Methods

Animal studies. Weaned, 3-week-old WT male C57BL/6 mice (The Jackson Laboratory) were fed isocaloric diets of either LP (2% protein, Teklad Lab Animal Diet, TD.110200; Harlan Laboratories) or RP (20% protein, Teklad Lab Animal Diet, TD.08678; Harlan Laboratories) for 8 to 15 days prior to infection, and then for 15 to 22 days after infection (LP groups), or for 22 to 64 days after infection (RP groups), as indicated in the Results section. All mice were maintained on antibiotics (vancomycin 1 mg/ml, Novaplus; neomycin 1.4 mg/ml, Durvet; and ampicillin 1 mg/ml, Sigma-Aldrich/Fischer Scientific) ad libitum in their drinking water (27). At 4 to 5 weeks of age, the mice were infected orogastrically with a 100-μl inoculum of either 10^7 *G. lamblia* WB trophozoites (assemblage A) in TYI-S-33 media or 10^6 purified *G. lamblia* H3 (assemblage B) cysts (Waterborne, Inc.) in PBS (55). The mice were weight-matched prior to initiation on the diets and again prior to infection. Postinfection weights were obtained serially for each individual mouse prior to sacrifice. The mice were administered ketamine-xylazine according to institutional protocol, and euthanization was confirmed with cervical dislocation prior to tissue harvest.

G. lamblia isolates. *G. lamblia* WB trophozoites (provided by S. Singer, Georgetown University) were cultured in TYI-S-33 media supplemented with 1 × antibiotic-antimycotic (15240-062; Invitrogen) and passed twice weekly. On the day of infection, 48-hour trophozoites were placed on ice for 30 minutes, centrifuged at 450 *g*, and resuspended in fresh ice-cold TYI-S-33 media (pH 7.4) (27). Commercially purified *G. lamblia* H3 cysts (Waterborne, Inc.) were an original human isolate from Colorado (H. Stibbs, Waterborne, Inc., personal communication). *G. lamblia* H3 cysts were received in antibiotic-antimycotic solution and stored at 4°C for a maximum of 1 week. On the day of infection, cysts were washed and resuspended in PBS and kept on ice prior to infection. Inoculation of the post-wash cyst supernatant onto sheeps' blood and MacConkey agar at 37°C revealed no growth at 24 hours.

Stool/tissue DNA extraction and real-time PCR of Giardia lamblia. Confirmation of live *G. lamblia* trophozoite detection ex vivo was performed on 4-cm segments of duodenum minced in ice-cold PBS and examined after 30 to 45 minutes (Supplemental Figure 1A), and the presence of *G. lamblia* cysts in the cecum was identified using immunofluorescence (Merifluor) in pooled cecal contents in 10% Zn-formalin according to the manufacturer's protocol (Supplemental Figure 1B). Stool, cecal contents, and intestinal tissue samples (0.5-cm segments each of duodenum [4 cm after the pylorus], jejunum [8 cm distal to the duodenal segment], and ileum [1 cm proximal to the cecum]), were homogenized, and DNA was extracted and purified using QIAmp DNA Mini Spin Columns (QIAGEN) either manually, similarly to a previous protocol (60), or with the use of a QIAcube auto-

mated instrument (QIAGEN). Real-time PCR for *G. lamblia* detection was performed using primer sequences for the 18S small ribosomal subunit (forward primer, 5′-GACGGCTCAGGACAACGGTT-3′ [Operon]; reverse primer, 5′-TTGCCAGCGGTGTCCG-3′ [Operon]; probe FAM-5′-CCCGC-GGCGGTCCCTGCTAG-3′-BHQ [IDT]) and IQSupermix (BioRad) supplemented with $MgCl_2$ (BioLabs) on a BioRad CFX iCycler according to previously published conditions (61). For quantification of parasite burden, DNA extraction and PCR assay were validated and optimized using known concentrations of *G. lamblia* H3 cysts spiked into 40-mg aliquots of pooled stool pellets from never-infected C57BL/6 mice. This concentration gradient served as a standard curve for every assay (Supplemental Figure 1C). Amplifications with cycle times (Ct) greater than 36 were considered nonspecific, and therefore Ct values greater than 36 cycles were excluded from analysis. Ct values for each sample were plotted relative to the standard curve and normalized to each respective stool or tissue weight. The reliable limit of detection was determined to be 1×10^3 parasites per gram of stool.

Microscopy, intestinal morphometry, and immunohistochemical staining. At the time of sacrifice, 1.5- to 2-cm segments of small bowel (duodenum [4 cm after the pylorus], jejunum [8 cm distal to the duodenal segment], and ileum [1 cm proximal to the cecum]) were fixed in 10% Zn-formalin, transferred to 70% EtOH prior to paraffin embedding, and then stained with H&E. Villus length and crypt depth measurements were recorded only on full-length villi with adjacent crypts, defined as a "villus-crypt unit" (7–15 villi per mouse) (Image J software; NIH) and read in a blinded manner (L.A. Bartelt and J. Roche). Eosinophil morphology was confirmed on a subset of tissues using Congo red stain (62). Rabbit anticleaved caspase-3 antibody staining was performed using a DAKO auotostainer with a hematoxylin counterstain according to protocol. Eosinophils and cleaved caspase-3 positivity were independently quantified in a blinded manner under ×20 and ×40 magnification with criteria including a full villus-crypt unit, no adjacent lymphoid aggregates, cellular morphology characterized by either large red granules or clearly bilobed nuclei on H&E staining for eosinophils (S. Zaja-Milatovic and L.A. Bartelt), and either cytoplasmic or nuclear staining for cleaved caspase-3 positivity (C. Warren and L.A. Bartelt).

Duodenal tissue cytokine mRNA analysis. Total RNA was extracted using an RNeasy Mini kit (QIAGEN). Each tissue sample was suspended in 350 μl of RLT lysis buffer and incubated at room temperature for 2 hours to soften the tissues. Then an equal volume of 70% ethanol was added to the samples and they were homogenized by centrifugation through QIAGEN QIAshredder columns. The homogenized samples were applied to RNeasy Mini columns (QIAGEN) and processed according to the manufacturer's instructions. In order to remove the genomic DNA carried over from RNA extraction, DNase I (Ambion) treatment was performed following the manufacturer's instructions. Reverse transcription was then performed with MultiScribe reverse transcriptase (Applied Biosystems) using random hexamers according to the manufacturer's instructions. For each gene examined, primers were designed from the target sequences retrieved from the RefSeq Sequence Database (http://www.ncbi.nlm.nih.gov/RefSeq/) using Primer Express 3.0 software (Applied Biosystems) and synthesized according to the manufacturer's instructions (Invitrogen) (Supplemental Table 1). Selection of the primers was performed according to the suggested recommendations, but was tailored to best fit the requirement of the SYBR Green assays. The perspective assay was validated and optimized before applying the results to the experimental samples. Quantitative PCRs (qPCRs) were carried out in triplicate using equal amounts of each cDNA sample, which was approximately equivalent to 50 ng of starting total RNA. Power SYBR Green Master Mix (BioRad) was used with the respective forward and reverse primers at the optimized concentrations in a total volume of 25 μl. PCR amplification and fluorescent emission monitoring in real time were performed using the ABI Prism 7900HT Sequence Detection System (Applied Biosystems) as described in the ABI SYBR Green protocol. To verify that only a single PCR product was amplified per transcript, dissociation curve data were analyzed with 7900HT Sequence Detection Software (Applied Biosystems). To account for differences in starting material, qPCR was also performed for each cDNA sample using housekeeping genes, mouse hypoxanthine-guanidine phosphoribosyltransferase and beta-actin, synthesized at our own facility. The data collected from these qPCRs defined a threshold cycle number (Ct) of detection for the target or the housekeeping genes in each cDNA sample. In order to convert the Ct values into a relative abundance of target and housekeeping genes per sample, a standard curve was generated for the housekeeping gene using serial dilutions of the cDNA sample. An arbitrary value of the template was first assigned to the highest standard, then corresponding values were assigned to the subsequent dilutions, and these relative values were plotted against the Ct value determined for each dilution, resulting in the generation of the standard curve. The relative amount of target and housekeeping genes in each sample was then determined using the comparative Ct method as described (63). The relative quantity (RQ) of target, normalized to an endogenous reference (usually a housekeeping gene) and relative to a calibrator (the Rox reference dye in this case), was calculated by: $RQ = 2^{-\Delta\Delta Ct}$, where ΔΔCt represents the difference in Ct between the transcript and the housekeeping gene for the same RNA sample. The ratio of the RQs for the treated sample and the experiment sample were used to derive the fold change. ANOVA was then used to determine the mean and standard error of the mean for each comparison.

Flow cytometry. Suspensions of small intestinal epithelial and lamina propria cells were prepared from 8-cm segments of small intestine beginning 8 cm distal to the pyloric sphincter. After segments were PBS-flushed and cleaned of gross debris and mucus, they were incubated at 37°C in a 50-mM EDTA, 1-mM DTT, HBSS buffer for 1 hour in a shaking incubator. The resulting supernatant containing the epithelial cells was collected and filtered through a 70-μm cell filter and placed immediately on ice. For lamina propria cell isolations, the remaining tissue pieces were minced and suspended in 10 ml RPMI media containing 0.17 mg/ml liberase TL, and 30 μg/ml DNase enzyme solution for 1 hour at 37°C in a shaking water bath. The digested pieces were strained serially through a 100-μm filter and a 40-μm filter. The resulting pellets were resuspended in 10% FCS-PBS buffer. Fluorophore-conjugated purified mAbs used in flow cytometry were purchased from BD Biosciences (CD8-FITC, CD4-PE, Siglec F-PE, CD45-V500, and CD11b-FITC) and Biolegend (B220 [CD45R]-PerCP), and cell surface staining was performed according to the manufacturer's instructions. All samples were acquired on a CyAn ADP LX analyzer (BD Biosciences and Cytek Development) and analyzed with FlowJo version 9.3.3 software (Tree Star).

Statistics. Statistics were performed using GraphPad Prism 5.0c (GraphPad Software). For growth curves and serial stool shedding, 2-way ANOVA and a Bonferonni's post test analysis with repeated measures were used. Data in the growth and scatter plots represent the means ± SEM. qPCR data were log transformed for statistical comparisons. For parameter comparisons between groups, an unpaired Student's *t* test or 1-way ANOVA was used when appropriate. *P* values of less than 0.05 were considered significant.

Study approval. Mouse study protocols were approved by the IACUC of the University of Virginia (protocol 3315-08-09).

Acknowledgments

This work was supported in part by the following NIH grants: R01 HD053131 and U01 AI057168 (to R.L. Guerrant); U01 AI 075520 (to P. Hoffman); T32 DK007769-11 (to L.A. Bartelt); and AI 094492-01 (to S. Singer). We thank Snjezana Zaja-Milatovic, Shahram Solaymani-Mohammadi, Carol Gilchrist, Mami Taniuchi, and Suzanne Stroup for laboratory and technical support;

Y. Bao and the University of Virginia Biomolecular Research Facility for tissue RNA extraction, cDNA construction, and mRNA quantification; P. Pramoonjago and the Biorepository and Tissue Research Facility of the University of Virginia for immunhistochemical staining; and Eric Houpt, Rebecca Dillingham, and William Petri for experimental design guidance.

Received for publication October 15, 2012, and accepted in revised form March 15, 2013.

Address correspondence to: Luther A. Bartelt, Infectious Diseases, University of Virginia, Charlottesville, Virginia 22903, USA. Phone: 434.924.5242; Fax: 434.924.0075; E-mail: lab2za@virginia.edu.

1. Ali SA, Hill DR. Giardia intestinalis. *Curr Opin Infect Dis*. 2003;16(5):453–460.
2. Savioli L, Smith H, Thompson A. Giardia and Cryptosporidium join the 'Neglected Diseases Initiative'. *Trends Parasitol*. 2006;22(5):203–208.
3. Mondal D, et al. Contribution of enteric infection, altered intestinal barrier function, and maternal malnutrition to infant malnutrition in Bangladesh. *Clin Infect Dis*. 2012;54(2):185–192.
4. Hill DR, Nash TE. Giardia lamblia. In: Mandell GL, Bennett JE, Dolin R, eds. *Principles and Practices of Infectious Diseases*. 5th ed. Philadelphia, Pennsylvania, USA: Churchill Livngstone Elsevier; 2009:3527–3534.
5. Newman RD, Moore SR, Lima AA, Nataro JP, Guerrant RL, Sears CL. A longitudinal study of *Giardia lamblia* infection in north-east Brazilian children. *Trop Med Int Health*. 2001;6(8):624–634.
6. Lima AA, et al. Persistent diarrhea signals a critical period of increased diarrhea burdens and nutritional shortfalls: a prospective cohort study among children in northeastern Brazil. *J Infect Dis*. 2000; 181(5):1643–1651.
7. Al-Mekhlafi MS, et al. Giardiasis as a predictor of childhood malnutrition in Orang Asli children in Malaysia. *Trans of the R Soc of Tropl Med and Hyg*. 2005; 99(9):686–691.
8. Botero-Garcés JH, et al. Giardia intestinalis and nutritional status in children participating in the complementary nutrition program, Antioquia, Colombia, May to October 2006. *Rev Inst Med Trop São Paulo*. 2009;51(3):155–162.
9. Nematian J, Gholamrezanezhad A, Nematian E. Giardiasis and other intestinal parasitic infections in relation to anthropometric indicators of malnutrition: a large, population-based survey of schoolchildren in Tehran. *Ann of Trop Med and Parasitol*. 2008;102(3):209–214.
10. Hollm-Delgado MG, et al. Lack of an adverse effect of *Giardia intestinalis* infection on the health of Peruvian children. *AmJ Epidemiol*. 2008;168(6):647–655.
11. Goto R, Mascie-Taylor NCG, Lunn PG. Impact of intestinal permeability, inflammation status and parasitic infections on infant growth faltering in rural Bangladesh. *Br J Nutr*. 2009;101(10):1509–1516.
12. Goto R, Mascie-Taylor NCG, Lunn PG. Impact of anti-*Giardia* and antihelminthic treatment on infant growth and intestinal permeability in rural Bangladesh: a randomized double-blinded controlled study. *Trans R Soc Trop Med Hyg*. 2009; 103(5):520–529.
13. Simsek Z, Zeyrek FY, Kurcer MA. Effect of *Giardia* infection on growth and psychomotor development in children aged 0–5 years. *J Trop Pediatr*. 2004; 50(2):90–93.
14. Ajjampur SS, et al. Effect of cryptosporidial and giardial diarrhea on social maturity, intelligence and physical growth in children in a semi-urban slum in south India. *Ann Trop Paediatr*. 2011; 31(3):205–212.
15. Berkman DS, Lescano AG, Gilman RH, Lopez SL, Black MM. Effects of stunting, diarrheal disease, and parasitic infection during infancy on cognition in late childhood: a follow-up study. *Lancet*. 2002; 359(9306):564–571.
16. Lunn PG, Erinoso HO, Northrop-Clewes CA, Boyce SA. *Giardia intestinalis* is unlikely to be a major cause of the poor growth in rural Gambian infants. *J Nutr*. 1999;129(4):872–877.
17. Prado MS, Cairncross S, Strina A, Barreto ML, Oliveira-Assis AM, Rego S. Asymptomatic giardiasis and growth in young children; a longitudinal study in Salvador Brazil. *Parasitol*. 2005;131(pt 1):51–56.
18. Veenemans J, et al. Protection against diarrhea associated with Giardia intestinalis is lost with multi-nutrient supplementation: a study in Tanzanian children. *PLoS Negl Trop Dis*. 2011;5(6):e1158.
19. Mondal D, Haque R, Sack RB, Kirkpatrick BD, Petri WA. Attribution of malnutrition to cause-specific diarrheal illness: evidence from a prospective study of preschool children in Mirpur, Dhaka, Bangladesh. *Am J Trop Med Hyg*. 2009;80(5):824–826.
20. Quihui-Cota L, Astiazarán-García H, Valencia ME, Morales-Figueroa GG, Lopez-Mata MA, Vazquez Ortiz F. Impact of *Giardia intestinalis* on vitamin A status in schoolchildren from northwest Mexico. *Int J Vitamin Nutr Res*. 2008;78(2):51–56.
21. Quihui L, Morales GG, Méndez RO, Leyva JG, Esparza J, Valencia ME. Could giardiasis be a risk factor for low zinc status in schoolchildren from northwestern Mexico? A cross-sectional study with longitudinal follow-up. *BMC Public Health*. 2010;10(1):85.
22. Rosado JL, et al. Interaction of zinc or vitamin A supplementation and specific parasite infections on Mexican infants' growth: a randomized clinical trial. *Eur J Clin Nutr*. 2009;63(10):1176–84.
23. Cook DM, Swanson RC, Eggett DL, Booth GM. A retrospective analysis of prevalence of gastrointestinal parasites among school children in the Palajunoj Valley of Guatemala. *J Health Popul Nutr*. 2009; 27(1):31–40.
24. Goto R, Panter-Brick C, Northrop-Clewes CA, Manahdhar R, Tuladhar NR. Poor intestinal permeability in mildly stunted Nepali children: associations with weaning practices and *Giardia lamblia* infection. *Br J Nutr*. 2002;88(2):141–149.
25. Muhsen K, Levine MM. A systematic review and meta-analysis of the association between *Giardia lamblia* and endemic pediatric diarrhea in developing countries. *Clin Infect Dis*. 2012;55(suppl 4):S271–S293.
26. Singer SM, Nash TE. T-cell-dependent control of acute *Giardia lamblia* infections in mice. *Infect Immun*. 2000;68(1):170–175.
27. Solaymani-Mohammadi S, Singer SM. Host immunity and pathogen strain contribute to intestinal disaccharidase impairment following gut infection. *J Immunol*. 2011;187(7):3769–3775.
28. Li E, Zhao A, Shea-Donohue T, Singer SM. Mast cell-mediated changes in smooth muscle contractility during mouse giardiasis. *Infect Immun*. 2004; 75(9):4514–4518.
29. Leitch GJ, Udezulu IA, He Q, Visvesvara GS. Effects of protein malnutrition on experimental giardiasis in the mongolian gerbil. *Scand J Gastroenterol*. 1993;28(10):885–893.
30. Shukla G, Sidhu RK. *Lactobacillus casei* as a probiotic in malnourished *Giardia lamblia*-infected mice: a biochemical and histopathological study. *Can J Microbiol*. 2011;57(2):127–135.
31. Roche JK, Cabel A, Sevilleja J, Nataro J, Guerrant RL. Enteroaggregative *Escherichia coli* (EAEC) impairs growth while malnutrition worsens EAEC infection: a novel murine model of the infection malnutrition cycle. *J Infect Dis*. 2010;202(4):506–514.
32. Coutinho BP, et al. *Cryptosporidium* infection causes undernutrition and, conversely, weanling undernutrition intensifies infection. *J Parasitol*. 2008; 94(6):1225–1232.
33. Costa LB, et al. Cryptosporidium-malnutrition interactions: mucosal disruption, cytokines, and TLR signaling in a weaned murine model. *J Parasitol*. 2011;97(6):1113–1120.
34. Costa LB, et al. Novel in vitro and in vivo models and potential new therapeutics to break the vicious cycle of cryptosporidium infection and malnutrition. *J Infect Dis*. 2012;205(9):1464–1471.
35. Farthing MJ, Mata L, Urrutia JJ, Kronmal RA. Natural history of *Giardia* infection of infants and children in rural Guatemala and its impact on physical growth. *Am J Clin Nutr*. 1986;43(3):395–405.
36. Byrd LG, Conrad JT, Nash TE. *Giardia lamblia* infections in adult mice. *Infect Immun*. 1994;62(8):3583.
37. Zhou P, Li E, Zhu N, Robertson J, Nash T, Singer SM. Role of interleukin-6 in the control of acute and chronic *Giardia lamblia* infections in mice. *Infect Immun*. 2003;71(3):1566–1568.
38. Chin AC, Teoh DA, Scot KG, Meddings JB, Macnaughton WK, Buret AG. Strain-dependent induction of enterocyte apoptosis by *Giardia lamblia* disrupts epithelial barrier function in a caspase-3-dependent manner. *Infect Immun*. 2002;70(7):3673–3680.
39. Troeger H, et al. Effect of chronic *Giardia lamblia* infection on epithelial transport and barrier function in human duodenum. *Gut*. 2007;56(3):328–335.
40. Koot BG, ten Kate FJ, Juffrie M, Rosalina I, Taminiau JJ, Benninga MA. Does *Giardia lamblia* cause villous atrophy in children?: a retrospective cohort study of the histological abnormalities in giardiasis. *J Pediatr Gastroeneterol Nutr*. 2009;49(3):304–308.
41. Long KZ, et al. Associations between mucosal innate and adaptive immune responses and resolution of diarrheal pathogen infections. *Infect Immunol*. 2010;78(3):1221–1228.
42. Cunningham-Rundles S, Lin DH. Nutrition and the immune system of the gut. *Nutrition*. 1998; 14(7–8):573–579.
43. Koster F, Pierce NF. Effect of protein deprivation on immunoregulatory cells in the rat mucosal immune response. *Clin Exp Immunol*. 1985;60(1):217–224.
44. Upadhyay P, Ganguly NK, Walia BN, Mahajan RC. Kinetics of lymphocyte subpopulation in intestinal mucosa of protein deficient *Giardia lamblia* infected mice. *Gut*. 1986;27(4):386–391.
45. Matowicka-Karna J, Kralisz M, Kemona H. Assessment of the levels of nitric oxide (NO) and cytokines (IL-5, IL-6, IL-13, TNF, IFN-gamma) in giardiasis. *Folia Histochem Cytobiol*. 2011;49(2):280–284.
46. Hagel I, et al. Co-infection with *Ascaris lumbricoides* modulates protective immune responses against *Giardia duodenalis* in school Venezuelan rural children. *Acta Trop*. 2011;117(3):189–195.
47. Kamda JD, Singer SM. Phosphoinositide 3-kinase-dependent inhibition of dendritic cell interleukin-12 production by *Giardia lamblia*. *Infect Immun*. 2009;77(2):685–693.
48. Chatterjee A, et al. *Giardia* cyst wall protein 1 is a lectin that binds to curled fibrils of the GalNAc homopolymer. *PLoS Pathog*. 2010;6(8):e1001059.
49. Jimenez JC, Fontaine J, Grzych JM, Dei-Cas E, Capron M. Systemic and mucosal responses to oral administration of excretory and secretory antigens from *Giardia intestinalis*. *Clin Diagn Lab Immunol*. 2004;11(1):152–160.
50. Panaro MA, et al. Caspase-dependent apoptosis of the HCT-8 epithelial cell line induced by the parasite *Giardia intestinalis*. *FEMS Immunol Med Microbiol*. 2007;51(2):302–309.

51. Stadelmann B, Merino MC, Persson L, Svärd SG. Arginine consumption by the intestinal parasite *Giardia intestinalis* reduces proliferation of intestinal epithelial cells. *PLoS One*. 2012;7(9):e45325.
52. Solaymani-Mohammadi S, Singer SM. Regulation of intestinal epithelial cell cytoskeletal remodeling by cellular immunity following gut infection. *Mucosal Immunol*. 2013;6(2):369–378.
53. Cliffe LJ, Humphreys NE, Lane TE, Potten CS, Booth C, Grencis RK. Accelerated intestinal epithelial cell turnover: a new mechanism of parasite expulsion. *Science*. 2005;308(5727):1463–1465.
54. Solaymani-Mohammadi S, Singer SM. *Giarida duodenalis*: the double-edged sword of immune responses in giardiasis. *Exp Parasitol*. 2010; 126(3):292–297.
55. Guy RA, Payment P, Krull UJ, Horgen PA. Real-time PCR for quantification of *Giardia and Cryptosporidium* in environmental water samples and sewage. *Appl Environ Microbiol*. 2003;69(9):5178.
56. Li D, Craik SA, Smith DW, Belosevic M. Comparison of levels of inactivation of two isolates of *G. lamblia* cysts by UV light. *Appl Environ Microbiol*. 2007; 73(3):2218–2223.
57. Hill DR, Guerrant RL, Pearson RD, Hewlett EL. *Giardia lamblia* infection of suckling mice. *J Infect Dis*. 1983;147(2):217–221.
58. Singer SM, Nash TE. The role of normal flora in *Giardia lamblia* infections in mice. *J Infect Dis*. 2000; 181(4):1510–1512.
59. Nash TE, Herrington DA, Losonosky GA, Levin MM. Experimental human infections with *Giardia lamblia*. *J Infect Dis*. 1987;156(6):974–984.
60. Parr JB, et al. Detection and quantification of *Cryptosporidium* in HCT-8 cells and human fecal specimens using real-time polymerase chain reaction. *Am J Trop Med Hyg*. 2007;76(5):938–942.
61. Haque R, et al. Multiplex real-time PCR assay for detection of *Entamoeba histolytica*, *Giardia intestinalis*, and *Cryptosporidium spp*. *Am J Trop Med Hyg*. 2007; 76(4):713–717.
62. Meyerholz DK, Griffin MA, Castilow EM, Varga SM. Comparison of histochemical methods for murine eosinophil detection in an RSV vaccine-enhanced inflammation model. *Toxicol Pathol*. 2009; 37(2):249–255.
63. *User Bulletin 2: Relative Quantitation of Gene Expression*. Applied Biosystems; 2001.